Study of a row of jets impinging a concave wall by classic and stereoscopic PIV

Laurent-Emmanuel BRIZZI[1], Virginie GILARD[2]

1: Laboratoire d'Etudes Aérodynamiques, Université de Poitiers, Poitiers, France, Laurent.brizzi@lea.univ-poitiers.fr
2: Laboratoire d'Etudes Aérodynamiques, Université de Poitiers, Poitiers, France, Virginie.gilard@lea.univ-poitiers.fr

Abstract The aerodynamic study of a row of round jets impinging a concave wall is carried out from velocity measurements obtained by the standard and stereoscopic Particle Image Velocimetry.
The present work extends a previous study of a two-dimensional jet impinging a concave wall. It deals with a more complex case, found in practical applications, namely a line of five round jets impinging a concave wall. This flow is described from the average velocity fields and turbulent values obtained by Particle Image Velocimetry (PIV). To better understand the global structure and characteristics of this three-dimensional flow, the stereoscopic PIV (SPIV) is also used. This recent technique allows simultaneous measurements of the three velocity components extracted from two different views of the same flow region. The principle and the specific aspects of the stereoscopic PIV set up are then explained.
After a statistical data processing, the three-dimensional structure and the characteristics of multiple jets impinging a concave wall are described with the mean velocity fields and the turbulent values in several planes of the flow.
Results indicate that the flow structure of several round jets impinging a concave wall has features in common with the multiple jets impacting a plane wall. However, when the jet meets a concave surface, one observes the formation of a swirl stabilizing around the stagnation zone. In spite of a delicate set up made by the concave form of the impingement surface, results obtained by SPIV make it possible to confirm the three-dimensional structure and the interaction between the jets issuing from a line of jets impinging a concave wall.

1. Introduction

The impinging jets are widely used today in industry because they generate important heat and/or mass transfers. We find them in such applications as the drying of paper, textile, and ceramics but also for the cooling of electronic components or turbine blades. According to the applications, the conditions of impact differ and are defined by many geometrical or dynamic parameters.
Knowing the effects of these parameters on the heat transfer is necessary for good cooling system development. Although many research concentrated on the various parameters, certain gaps remain concerning the shape of the impinged wall. Indeed, the majority of the studies relate to a unique (or several) jet impinging a plane wall. For the cooling of the turbine blade internal surface, the curvature along the semi-cord is so low that we can, at first approximation, consider that the jets impact a plane wall. This assumption is not true at the leading edge where the jets impact a concave curved surface. Unfortunately, only very few studies relate to curved walls (about fifteen during the last 30 years). Moreover, it is the thermal aspect of the impinging jets which is more largely studied because of their many applications even if the thermal and aerodynamic aspects are strongly dependent.
Thus until in the Eighties, the main part of the studies relates to the thermal aspect analysis of thermal correlations Nu=f(Re) [1-3]. In the Eighties, the first pressure measurements appear [4-5], then in the Nineties the interest is mostly on the visualization of the physical phenomena [6-7]. It is only recently that some studies relate to the aerodynamic field of the flow induced by impinging jets on a curved wall [8-10]. After the study of a slot jet impinging a concave wall [10], we were

interested in the more complex case, but also the more used in industry: a line of round jets impinging a concave wall. This flow field is described from the average velocity fields and turbulent values obtained by Particles Image Velocimetry (PIV). In order to highlight more details on the structure and the characteristics of this three-dimensional flow, stereoscopic PIV was also used.

2. Experimental device

The five jets originate from 10 mm inner diameter (d) circular tubes drowned in an Altuglas block (30 mm thickness, 20 mm length and 310 mm width, *cf*. Figure 1). The distance between two jets (p) is fixed at 40 mm (p/d=4). The same velocity U_j is applied to each jet by means of a device that includes a fan, a distributor, valves and venturi (not presented on figure 1). The transparent impingement surface consists of a half cylinder (internal diameter C_d of 52 mm), forming the concave part of the target, and two plates fixed in prolongation of the half cylinder edges and used as upper and lower boundaries (*cf*. Figure 1). It is closed laterally by two buffer plates (not presented on figure 1).
The main parameters of our study are the Reynolds number ($Re_d=U_j.d/\nu$), the impinging height H/d (H is the distance between the jet exit and the wall) and the relative curvature D_c/d (*cf*. Figure 1). For this study, the configuration ($Re_d=6400$; H/d=7; $D_c/d=5.2$) was retained in order to describe the flow structure. The flow temperature is maintained constant by means of a thermal regulator.

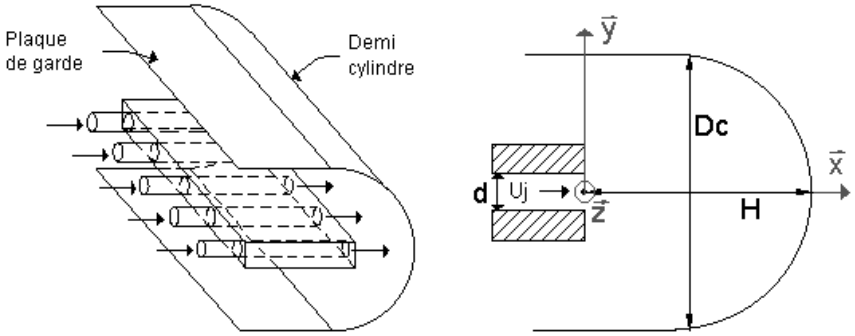

Figure 1 : Diagram a line of five round jets and the main plane of the study.

3. Classic and Stereoscopic PIV

Stereoscopic PIV is a method for extracting the third, out-of-plane, velocity component from two cameras and is based on the principle of parallax [11]. In PIV, by placing two cameras so they observe the light-sheet plane from two different angles, the parallax effect means that you obtain slightly different two-velocity component vector maps from each camera.

The target consists of a plate on which points are ordered according to a reference mark and whose origin and axes are known.
Calibration begins with the frame grabbing of the target by each camera in various planes according to the direction perpendicular to the LASER sheet. The calibration relation between the image plane and the three-dimensional physical space for the two cameras is calculated by comparing the positions of the target points in various planes [13]. This calibration relation makes it possible thereafter to go from the two-dimensional velocity fields obtained by standard PIV to the three-

dimensional velocity flow field. Acquisitions of the images of the cameras were carried out using the software FlowManager 3.0.

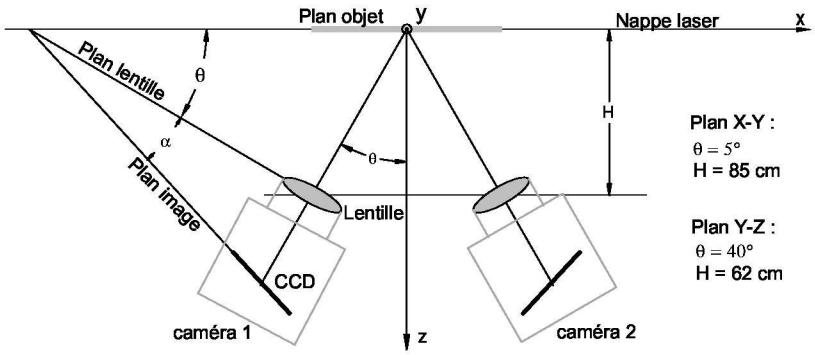

Figure 2 : Geometrical configuration (angular displacement system).

The two important steps of this measurement method are the acquisition of the two-dimensional velocity fields for each camera and the three-dimensional reconstitution making it possible to determine the three velocity components. Since standard PIV is a technique usually used nowadays, only the more specific parts related to the stereoscopic PIV will be presented (angular displacement configuration [12] and the rebuilding based on a three-dimensional calibration). The calibration of the two cameras was carried out using a two-dimensional target moving in the light sheet.
The adjustments of the parameters of measurement of the software are carried out in the same way has that for classic measurements by 2D2C PIV (adaptive Method four steps doubled into final: final window 32x32, overlap : 50x50%).
The measuring accuracy was estimated by relocating the target in Z-direction with a known and regular step and by determining the differences between the real displacements (Xr, Yr, Zr) and the displacements calculated by the software (Xm, Ym, Zm) from the target points. Table 1 gathers the average values (Δx, Δy, Δz) and the standard deviations (Ex, Ey, Ez) of the total errors on the three components for X-Y and Y-Z planes. Figure 3 presents, for X-Y plane, the mean and the standard deviation of the errors on the three components for various Z-planes as well as the space distribution of the error of the out of plane component.

a)

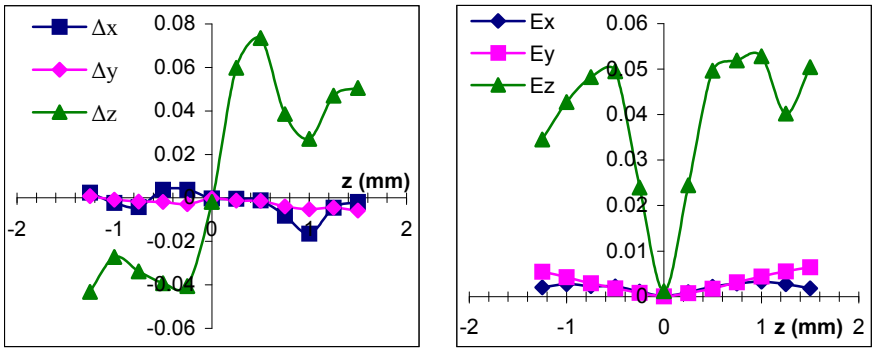

b)

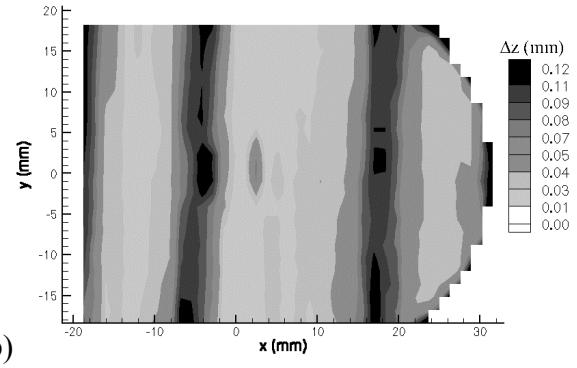

Figure 3 : Means and RMS values of the three components errors for several planes Z (a) and field of the z errors for the X-Y plane.

Stereoscopic PIV measurements provide the orthogonal velocity component of the measurement plane [11]. The method used for the SPIV measurements relies on the angular displacement configuration (*cf*. Figure 2) and the reconstruction based on a three-dimensional calibration [12]. These methods require additional precautions in association with traditional PIV adjustments.
The calibration of two cameras is carried out with a two-dimensional target moving in the light sheet. The target is a plate with ordered points according to a known reference pattern. The calibration begins with the acquisition of images of the target by each camera in various planes according to the z direction.
The relation of calibration between the three-dimensional image plane and the measured physical space for the two cameras is calculated by comparing the point positions of the target in the various planes [13]. From this calibration, it is possible in a second step to transform the two-dimensional velocity fields obtained by traditional PIV into a three-dimensional velocity field of the flow.
Image acquisitions by the cameras are carried out with the FlowManager 3.0 software. The PIV is evaluated by an adaptive multi pass correlation with a window size of 32x32 pixels and 50x50% overlap.
To evaluate the measurement accuracy, the target was moved in the out-plane direction with regular steps. The global errors can be estimated while defining the mean and RMS values of the difference between the real displacement and the reconstructed displacement of the target points (*cf*. Table 1 and Figure 3).

Global error (mm)	Δx	Ex	Δy	Ey	Δz	Ez
Plane X-Y	-0.002	0.002	-0.002	0.003	0.01	0.039
Plane Y-Z	0.147	0.054	-0.014	0.01	-0.02	0.01

Table 1 : Means and RMS values of the errors of the three components for the X-Y and Y-Z planes.

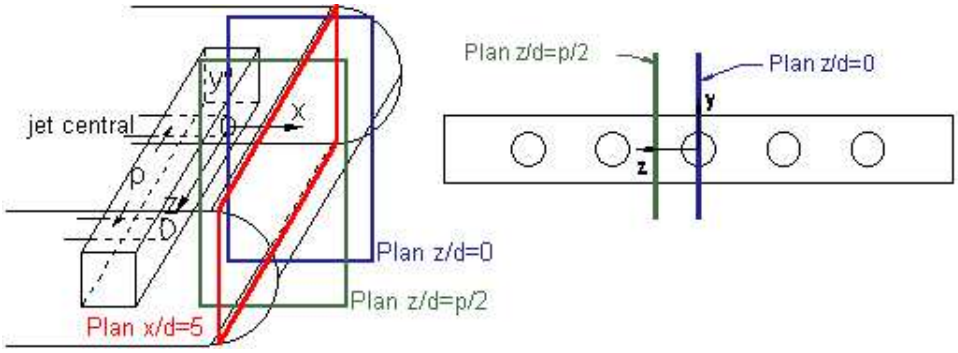

Figure 4: Plane positions for the study of a line of circular jets.

4. Results

The three-dimensional flow structure and the interaction between the jets are described by considering the measurements of the mean and turbulent velocity fields ($\sqrt{u'^2}$, $\sqrt{v'^2}$, $\sqrt{w'^2}$) obtained by standard and stereoscopic PIV. In order to examine the three-dimensional flow structure and the interaction between the jets several planes were retained (cf. Figure 4) :

- Two vertical planes X-Y located at z/d=0 (*i.e.* principal plane containing the jet axis) and at z/d=p/2 (median plane of two successive jets)
- One vertical plane Y-Z located at x/d=5.

For X-Y plans (z/d=0) and Y-Z (x/d=5), the stereoscopic PIV was used in order to obtain the three velocity components (U, V, W).

4.1 Flow structure of a round jet impinging a concave wall.

Figure 5 presents the mean velocity fields for X-Y planes at z/d=0 and z/d=p/2 (Re_d=6400; H/d=7; D_c/d=5.2). On these graphs we clearly observed that the jet impacts on the centre of the wall (x/d=7; y/d=0) (*cf.* Figure 5a). At the stagnation point, the jet separates and propagates in all directions. The presence of two vortices are also observed (*cf.* Figure 5b). They are located symmetrically with respect to the horizontal axis near x/d=5 and y/d=± 2.

In the round jet mixing layer, zone of strong shearing, some vortical structures are generated and then convected downstream. After the jet impact on the concave wall, these structures accumulate and form a swirl which seems to be stabilized at a distance s_t (curvilinear coordinate) of 3.3 d (about 70°) from the stagnation point (*cf.* Figure 5b). In fact it is a single structure which surrounds the impingement area. The centre of this vortex is located at a normal distance from the wall of approximately 0.8 d. This structure can be considered as the "ground vortex" observed in the case of jets impinging a plane wall with cross flow as mentioned by Barata [14].

In the transverse direction $\vec{z}$, this structure meets the corresponding vortex of the neighbour jet on the median plane of the two jets located at z/d=p/2. In this plane, the fluid leaves the wall and moves in the normal direction to the wall (cf. Figure 5c). This yields a "fountain effect" previously observed by Carcasci [15] and Saripalli [16] in the case of a circular jet impinging a plane wall.

For the X-Y plane at z/d=0, transverse component (W) iso-values are presented on figure 5a. However the W component values obtained by S-PIV seem largely overestimated (≈ 4 m/s) because of the low W values in this configuration (of the same order of magnitude as the vertical component ≈ 0.2 m/s) and the uncertainty of this component which is ten times higher compared to the in-plane

components. Moreover, taking into account the particular geometry of the experimental device, we could not get the most favourable conditions ($\theta = \pm 45°$). For the stereoscopic PIV, we thus had to use smaller angles ($\theta \approx 5°$ and $\theta \approx 40°$) which affect the precision.

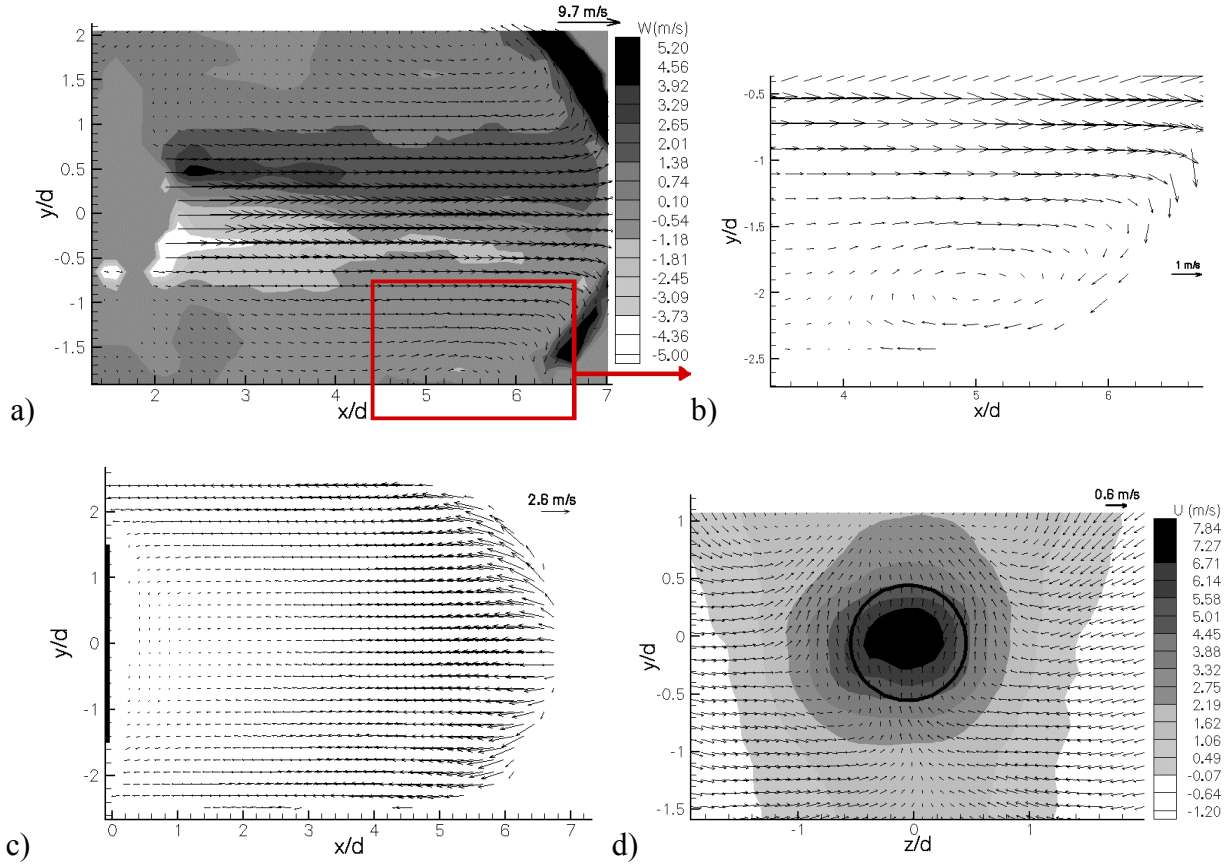

Figure 5: Mean velocity field for different planes X-Y at z/d = 0 (a and b), at z/d = p/2 (c) and plane Y-Z at x/d = 5 (d) (Re_d = 6400; H/d = 7; D_c/d = 5.2).

Figure 5d presents the mean velocity field and the longitudinal component U in Y-Z plane located at x/d=5. We clearly distinguish the round jet (central zone where the longitudinal component U is positive and maximum ≈ 7.84 m/s) and on the field edges (z/d=±2) zones where the U component is negative (U ≈ -1.2 m/s) corresponding to the fountain effect. We also notice, on the mean velocity field (V, W), the spread of the ambient fluid by the jet which seems to be done in a disordered way. However these velocities are not significant (V ≈ W << 1.5 m/s) and the average was only obtained from few instantaneous fields (n<1000).

4.2 Turbulent quantities.

The mean velocity fields and RMS values of the longitudinal (U) and vertical (V) velocity components are presented on figure 6 for the X-Y planes at z/d=0 and Y-Z plane at x/d=5. We observe on the various planes, that strong RMS values of the three components velocity are mainly located *in the jet mixing layer where various instabilities are characterized by swirling structures*

(Figures 6 and 7). In X-Y plane, the longitudinal fluctuations ($\sqrt{u'^2} \approx 0.15\ U_j$) are twice more important than the vertical fluctuations ($\sqrt{v'^2} \approx 0.08\ U_j$) (*cf.* Figure 6a). The values $\sqrt{w'^2}$ are strongly over-estimated ($\sqrt{w'^2} \approx 0.5\ U_j$) (*cf.* Figure 7) because of a higher uncertainty on the transverse component in the out of plane measurements coupled to a low value of the ratio between the W and U components. Indeed, the component W is given starting from U and the least error on this value automatically results in an error much more important for the transverse component W.

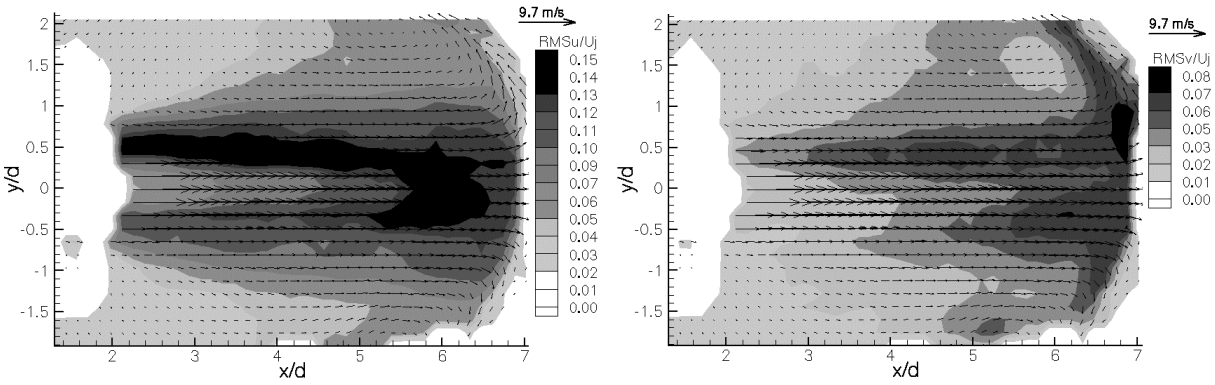

a) plane z/d = 0 (Plane X-Y)

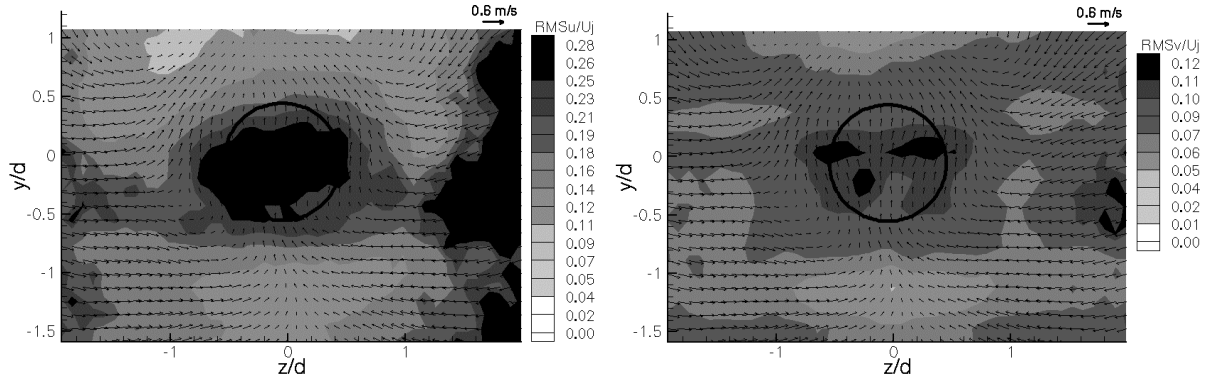

b) plane x/d = 5 (Plane Y-Z)

Figure 6: Mean velocity fields and $\sqrt{u'^2}$ and $\sqrt{v'^2}$ at different planes (Re_d=6400; H/d=7; D_c/d=5.2).

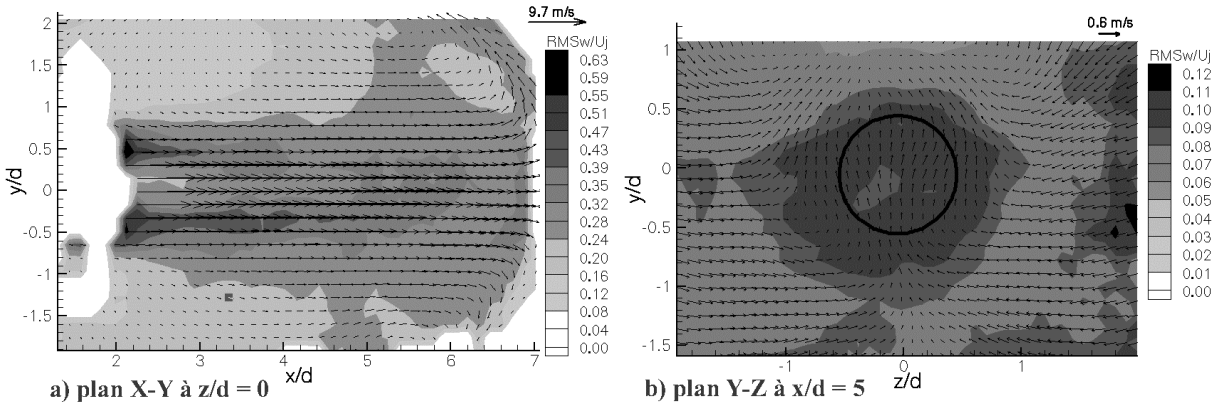

Figure 7: Mean velocity fields and $\sqrt{w'^2}$ *values at different planes (Re_d=6400; H/d=7; D_c/d=5.2).*

In addition, we observe that the zones of strong fluctuations of the longitudinal component ($\sqrt{u'^2}$) collapse in the centre of the jet near x/d=5, which corresponds to the end of the potential core of the jet (cf. Figure 6a). We notice then, as in the free jet case, a certain standardization of turbulence Indeed in Y-Z plane at x/b=5, the values $\sqrt{v'^2}$ and $\sqrt{w'^2}$ are about 0.12 U_j (cf. Figure 6b and 7b). The values $\sqrt{u'^2}$ are approximately 0.28 U_j and are overestimated but in this plane, the longitudinal component corresponds to the out-of plane component. However in X-Y plane at x/b=5, the value of $\sqrt{u'^2}$ is approximately 0.11 U_j.

In the vicinity of the stagnation point, we notice that the longitudinal fluctuations increase to reach their maximum value ($\sqrt{u'^2} \approx 0.14\ U_j$) at x/d≈6.4 and then decrease as the measurement point approaches the wall. Cooper et al. [17] also observed, in the case of a round jet impinging a plane wall, a reduction of the $\sqrt{u'^2}$ values approaching the wall at approximately 0.3 D from the wall. They explain this decrease by the decline of the turbulence diffusion starting from the mixing layer.

5. Conclusion

The results show that the flow structure of a row of round jets impinging on a concave wall has several common features with the multiple jets impinging a plane wall. We find strong RMS values of the three components velocity in the jet mixing layer, but also the fountain effect in the median plane of two successive jets. However when the jet impacts a concave surface, we observe the formation of a swirl stabilized around the stagnation zone. This study also allowed us to use and apprehend the technique of stereoscopic PIV.

In spite of a delicate set up made by the concave form of the impingement surface, results obtained by SPIV are encouraging and make it possible to confirm the three-dimensional structure and the interaction between the jets issuing from a line of jets impinging a concave wall.

References

[1] TABAKOFF W. & CLEVENGER W. , Gas turbine blade heat transfer augmentation by impingement of air jets having various configurations, ASME Journal of Engineering for Power

(1972) 51-60.
[2] METZER D.E., YAMASHITA T. & JENKINS C.W. , Impingement cooling of concave surfaces with lines circular air jets, ASME Journal of Engineering for Power (1969) 149-158.
[3] CHUPP R.E., HELMS H.E., McFADDEN P.W. & BROWN T.R. , Evaluation of internal heat transfer coefficients for impingement-cooled turbine airfoils, Journal of Aircraft 6 (1969) 203-208.
[4] LEE D.H., CHUNG Y.S. & WON S.Y. , The effect of concave surface curvature on heat transfer from a fully developed round impinging jet, Journal of Heat and Mass Transfer 42 (1999) 2489-2497.
[5] HRYCAK P. , Heat transfer from a row of impinging jets to concave cylindrical surfaces, Journal of Heat and Mass Transfer 24 (1981) 407-419
[6] CORNARO C., FLEISCHER A.S. & GOLDSTEIN J.R. , Flow visualisation of a round jet impinging on cylindrical surfaces, Experimental Thermal and Fluid Science 20 (1999) 66-78.
[7] GAU C. & CHUNG C.M. , Surface curvature effect on slot-air-jet impingement cooling flow and heat transfer process, Journal of Heat Transfer Transactions of ASME 113 (1991) 858-864.
[8] CHOI M., YOO H.S., YANG G., LEE J.S. & SOHN D.K. , Measurement of impinging jet flow and heat transfer on a semi-circular concave surface, Journal of Heat and Mass Transfer 43 (2000) 1811-1822.
[9] YANG G., CHOI M. & LEE J.S. , An experimental study of slot jet impingement cooling on concave surface : effects of nozzle configuration and curvature, International J. of Heat and Mass Transfer 42 (1999) 2199-2209.
[10] V. Gilard & L.-E. Brizzi, Slot jet impinging a curved wall, Proceedings of ASME Montreal (2002) n° FEDSM2002-31270.
[11] D. Calluaud, Développement d'une méthode de mesure tridimensionnelle par PIV stéréoscopique. Application à l'étude de l'écoulement naissant et établi autour d'un parallélépipède, (2003), Thèse de l'université de Poitiers.
[12] A.K. PRASAD, Stereoscopic particle image velocimetry, Experiments in Fluids 29 (2000) 103-116.
[13] S.M. Soloff, R.J. Adrian & Z.-C. Liu, Distortion compensation for generalized stereoscopic particle image velocimetry, Meas. Sci. Technol. 8 (1997) 1441-1454.
[14] BARATA J.M., Fountain flows produced by multiple impinging jets in a cross flow, AIAA Journal 34 (1996) 2523-2530.
[15] C. Carcasci, An experimental investigation on air impinging jets using visualisation methods, International J. Therm. Sci 38 (1999) 808-818.
[16] K.R. Saripalli, Visualisation of multi-jet impingement flow, AIAA Paper (1981) 81-1364.
[17] COOPER D., JACKSON D.C., LAUNDER B.E. & LIAO G.X., Impinging jet studies for turbulence model assessment I. Flow field experiments, Int. Journal of Heat and Mass Transfer 36 (1993) 2675-2684.